Advanced Steel Construction – Vol. 20 No. 3 (2024) 232–240
DOI:10.18057/IJASC.2024.20.3.3

STUDY ON THE ULTIMATE SHEAR PERFORMANCE OF CONCRET-FILLED STEEL TUBULAR COMPOSITE COLUMNS

Jian-Gang Wei [1, 2], Jin-Peng Han [1], Zhi-Tao Xie [1], Yan Yang [1] and Wei Zhang [2, 3, *]

[1] *College of Civil Engineering of Fuzhou University, No. 2, Wulongjiang Avenue, Minhou County, Fuzhou, Fujian, China.*
[2] *School of Civil Engineer, Fujian University of Technology, No. 33, Xuefu South Road, Minhou County, Fuzhou, Fujian, China.*
[3] *Institute of Theoretical and Applied Mechanics of the Czech Academy of Sciences Prosecká 809/76, 19000 Prague 9, Czech Republic.*
** (Corresponding author: E-mail: zhangwei621@gmail.com)*

ABSTRACT

The shear performance of three concrete-filled steel tubular (CFST) composite columns was investigated via single-point shear tests, considering shear-span ratios of 0.75, 1, and 1.5. The findings indicated that the failure mode of the CFST composite column transitioned from oblique compression shear failure to localized shear failure in the joint areas as shear-span ratio decreased. An extended analysis of the parameters was carried out utilizing the ABAQUS finite element model. The analysis indicates that the ultimate shear resistance capability of steel-concrete composite columns increases with the rise in the strength of the batten concrete, the batten concrete thickness-to-span ratio, and the outer diameter of column limbs. However, it decreases with an increase in shear-span ratio. The accuracy of the calculation methods for existing similar structures was assessed, and based on the force transmission mechanism of CFST composite columns, theoretical and simplified calculation methods were proposed that meet engineering precision requirements. Consequently, this method offers a valuable theoretical reference for engineering applications.

ARTICLE HISTORY

Received: 9 July 2023
Revised: 17 February 2024
Accepted: 20 February 2024

KEYWORDS

Concrete-filled steel tube;
Composite column;
Shear-span ratio;
Shear capability;
Calculation method

1. Introduction

Concrete-Filled Steel Tubular (CFST) composite columns consist of steel tube concrete limbs and concrete strips. In comparison to the steel-filled tubes of lattice columns, the higher stiffness of concrete strips in CFST composite columns leads to superior mechanical performance [1-4].

Currently, scholars have gradually conducted research on CFST composite columns and similar structures. Ou *et al.* [5] performed a comparative investigation into the axial and eccentric compression behavior of CFST composite short columns in contrast to lattice short columns. The findings unveiled the superior compressive strength, flexural rigidity, and load-carrying capability of CFST composite columns when juxtaposed with lattice columns. Furthermore, it was observed that the load-carrying capability of CFST composite columns exhibited constancy irrespective of variations in eccentricity ratio and slenderness ratio.

Xiong *et al.* [6-8] utilized double-layer parallel steel plates as connecting plates, conducting axial compression and lateral loading tests on equal or unequal limbs. The results indicated that compared to CFST columns with single steel plate connections, the double-plate CFST columns exhibited significantly improved load-carrying capability, stability, and lateral stiffness, demonstrating excellent deformation resistance capabilities.

Yong *et al.* [9] conducted pseudo-static tests on Reinforced Concrete (RC) frame-truss composite walls (FTCW). The results revealed that the most effective way to augment the load-bearing capability of RC frame-FTCW is by increasing the number of internal filled FTCW, followed by increasing the reinforcement ratio of the frame columns. The impact of escalating axial compression ratio, concrete strength, or introducing angle steel to the internal diagonal bracing in FTCW on the load-bearing capability is relatively negligible.

Quasi-static and quasi-dynamic tests were conducted on CFST composite columns by Yadav *et al.* [10-12], demonstrating their excellent seismic performance and complete hysteretic curves, which were similar to those observed in lattice columns. Nevertheless, the failure mode of the composite columns underwent a transformation, marked by the occurrence of concrete slab cracking and steel tube tearing.

Zhou et al. [13] undertook a seismic performance investigation involving six composite shear walls. The investigation explored the impact of axial load ratio, load eccentricity on the ductility and stiffness. Building upon these findings, Zhou introduced a shear force calculation methodology aligned with the precision criteria of engineering standards.

Zhang et al. [14] conducted a seismic performance study on five precast concrete-encased carbon fiber reinforced CFST composite walls with twin steel tube connections. The findings indicated that optimizing the wall with C100 steel fiber-reinforced high-strength concrete, as opposed to the reference wall using C80 concrete, led to improvements in structural load-bearing capability, deformation characteristics, and energy dissipation capability. The incorporation of bottom dual-layered steel plates to the high-strength concrete web constrained the web, augmenting deformation capability, while alleviating stiffness degradation and enhancing reparability.

CFST composite columns are frequently employed as bridge piers in various bridges across China [15-18]. However, these bridge piers are susceptible to shear failure induced by seismic events or collisions with vehicles or vessels. Therefore, the investigation of the shear behavior of CFST composite columns is of paramount importance [19]. Currently, scholars both domestically and internationally focus their research on CFST composite columns and similar structures primarily in terms of axial compression, lateral loading, and seismic behavior. The research on the shear performance of CFST composite columns and similar structures is relatively lacking, and the theoretical studies in this area are not comprehensive enough.

Wang *et al.* [20] compares RC filled CPSW with different connectors and axial compression ratios to RC shear walls. The results indicate a significant enhancement in shear capability for CPSW with CFSTs as boundary elements, compared to RC shear walls. Additionally, the study proposes a shear ultimate load-bearing capability calculation method that aligns with engineering precision requirements.

Liao [21] conducted theoretical derivations on the shear capability of CFST lattice columns. Based on the mechanism that the filled tube would not fail before the CFST lattice column, a shear capability calculation method applicable to lattice columns was proposed.

Nevertheless, the established shear capability calculation methods for analogous structures may not be universally applicable to CFST composite columns. Consequently, this paper entailed tests and analyses on three CFST composite columns with varying shear-span ratios. Subsequent to this, experimental data-validated finite element models were employed to conduct parameter expansion analyses. The purpose of these analyses was to examine the impact of various structural parameters, including the shear-span of ratio, thickness span ratio, batten concrete strength, and the outer diameter of the column limb, on the shear performance. Additionally, an evaluation of the accuracy of existing shear capability calculation methods for similar structures was conducted. Based on the force transmission mechanism of CFST composite columns, a study on the shear capability calculation methods for CFST composite columns was also undertaken.

2. Experimental program

2.1. Specimen design

The dimensions of the standard test specimen were established Derived from the lower half of the pier of the Ganhaizi bridge in Sichuan Province, specifically, the CFST composite columns. The dimensions were as follows: the column steel pipe measured 114 mm×2 mm, the longitudinal steel batten pipes were 48 mm×2 mm. The specimen's height was 1500 mm. The centroid of the column limb was located 300 mm from the longitudinal axis, while the batten pipes were spaced 150 mm vertically. The transverse batten consisted of a reinforced concrete slab with a width of b and thickness of 50 mm. This slab had embedded steel bars with diameters of 6 mm, spaced 50 mm vertically and 60 mm transversely. The transverse and longitudinal reinforcements of the reinforcement mesh were connected by binding, and the reinforcement mesh was attached to the column limbs via a connecting steel plate. The CFST composite column's shear-span ratio was adjusted by altering the height of the concrete batten b, with heights of 1000 mm, 750 mm, and 500 mm corresponding to shear-span ratios of 0.75, 1, and 1.5, respectively. The detailed diagram and specific parameters can be found in Fig. 1 and Table 1, respectively.

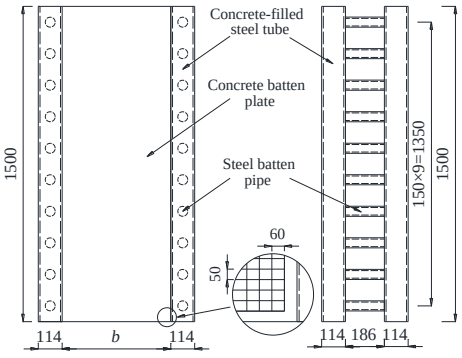

(a) The details of reinforcement

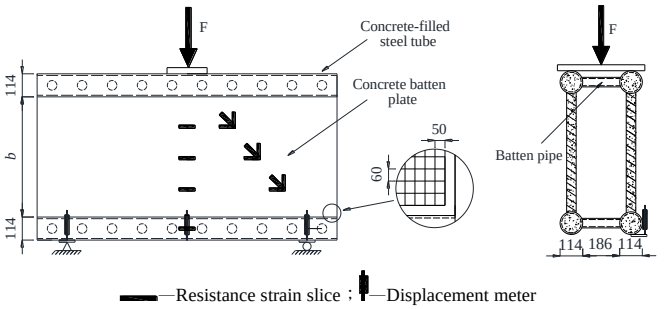

(b) Schematic diagram of test loading

(c) Field diagram of test loading

Fig. 1 Detail drawing of test loading device and specimen size

Table 1
Details of specimens

Specimen number	Height H/mm	Shear-span a/mm	batten plate width *b*/mm	Shear-span ratio λ	V_{Test}/kN	$V_{c\text{-}China}$/kN	$V_{c\text{-}simplify}$ /kN
S1-λ-0.75	1500	750	1000	0.75	621.6	1005.0	651.6
S2-λ-1			750	1	508.8	753.7	516.3
S3-λ-1.5			500	1.5	359.1	502.5	381.0

where S stands for the specimen, and the following values indicate the specimen type; λ=a/b, stands for shear-span ratio a and batten plate width b; Specimens are numbered according to specimen type - physical symbol of shear-span ratio - shear-span ratio value.

2.2. Material characteristics

The concrete and steel properties were tested according to the "Standard for test methods of mechanical properties on ordinary concrete" and "Metallic materials-Tensile testing Part 1: Method of test at room temperature", and the results are illustrated in Table 2.

Table 2
Material characteristics

Material	Elastic modulus *E*/GPa	f_y、f_c/MPa	f_t/MPa	Poisson's ratio μ
Steel pipe (columnar limb and batten pipe)	206	235	390	0.283
steel bar	198	321	519	0.3
Concrete (core concrete and batten concrete)	25.0	20.1	1.78	0.2

2.3. Loading method and instrumentation

The experiments were conducted on a 10000 kN hydraulic press at Fuzhou University. The test specimens were positioned on two support devices, with a steel block attached to the upper part of the specimen serving as the loading devices. During the tests, the specimens were subjected to loading through the upper loading device. The loading device and specimen size are illustrated in Fig. 2.

Initially, load control was implemented, employing a loading increment of 25 kN. Each successive load stage endured for a duration of 2-3 minutes to meticulously observe and document the mode and crack condition of the specimen. Subsequently, displacement loading, progressing at a rate of 0.2 mm/min, was employed until reaching the peak of the load curve, equivalent to 0.7 times the anticipated shear capability derived from the finite element method. Upon reaching this juncture, the loading procedure was terminated.

The arrangement of deformation measuring points is illustrated in Fig. 1(b). Displacement gauges were strategically located at both supports and the mid-span to monitor and document specimen deflection. Axial strain gauges were applied to the steel tube and concrete batten at the mid-span's bottom to gauge bending strain. Additionally, strain gauges were installed horizontally, vertically, and obliquely along the line connecting the loading point and supports on the concrete batten to measure shear strain.

3. Experimental results

3.1. Failure mode

In the initial loading phase, no noticeable alterations were detected on the specimen surfaces. Nevertheless, with the growing load, a multitude of slender and compact inclined cracks emerged in the concrete batten located between the loading point and the supports. These cracks exhibited an escalation in both width and quantity as the load intensified. Upon reaching its peak, the rate at which cracks widened and multiplied experienced a sudden acceleration, leading to continuous peeling off of the concrete at the loading point in the sectional specimens. As a result, the load could not be further increased, indicating that the composite column had reached its ultimate shear capability.

The ultimate failure mode diagram for each specimen is presented in Fig. 2. The concrete batten exhibited numerous diagonal cracks. In test S1-λ-0.75, where the shear-span ratio was minimal, the concrete batten near the loading point experienced tearing, while severe crushing and peeling off of concrete occurred at the junctions of reinforcement and upper column limbs. Test S2-λ-1 and S3-λ-1.5, which had larger shear-span ratios, exhibited more diagonal cracks than test S1-λ-0.75, albeit with less pronounced local failure characteristics of concrete spalling at the loading point or supports. The observed phenomenon suggests a shift in the failure mode of the CFST composite column from oblique compression shear failure to localized shear failure in the joint areas, correlating with a decrease in shear-span ratio.

(a) S1- λ -0.75

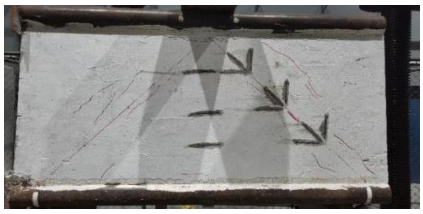

(b) S2- λ -1

(c) S3- λ -1.5

Fig. 2 Failure diagram of specimen

3.2. Load-deflection curve

The load-deflection (N-*f*) curve depicted in Fig. 3 for tests conducted under various shear-span ratios illustrates that, initially, the deflection of the middle span exhibited an approximately linear relationship with the load. This behavior indicates that the specimens were in the elastic stage during the early loading phase. Subsequently, prior to reaching 0.8 times the peak load, the deflection of the mid-span exhibited a nonlinear increase with the rising load, signaling the transition of the specimens into the elastic-plastic stage. After the load reached the peak value, the load will enter the stage of load-bearing capability decline. In the process of testing, the main failure mode of S2-*λ*-1 and S3-*λ*-1.5 was oblique compression and the shear capability decreased slowly, which showed the high residual load-bearing capability and ductility of these specimen. However, the capability of specimen S1-*λ*-0.75 decreased rapidly because it suffered local shear failure.

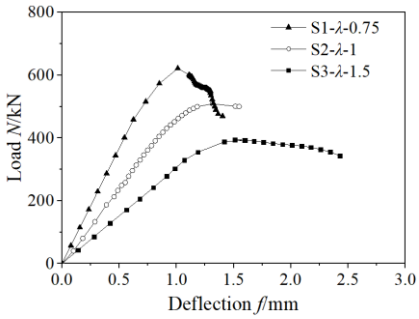

Fig. 3 Load-deflection curve

The load-deflection curves show that the initial slope and peak load of the curves were larger when shear-span ratio of the composite columns was smaller but the shear stiffness and ultimate shear capability were higher. Taking S3-*λ*-1.5 as the benchmark, the shear stiffness of S2-*λ*-1 and S1-*λ*-0.75 was increased by 237.5% and 462.5%, respectively and the shear capability of these specimens was increased by 28.9% and 57.5%, respectively.

3.3. Load-shear strain curve

The shear deformation at the midspan of the concrete batten was characterized by the most representative abdominal shear strain, and the load-strain curves are depicted in Fig. 4. The shear strain curves of the CFST composite columns exhibited linearity with the load during the initial loading stage, corresponding to the elastic stage of the specimens. In contrast, the shear strain curves of the concrete batten displayed a nonlinear relationship with the load, reaching approximately 0.8 times the peak value, marking the transition of the specimens into the elastic-plastic stage.

The shear strain curves of the specimens increased rapidly while the load approached the peak value, which indicated that the cracks of the concrete batten were in the unstable stage, and the shear deformation increased obviously. The shear force of specimens S2-*λ*-1 and S3-*λ*-1.5 can still be transferred from the column limb to the batten slab, although the force transfer mechanism of specimen S1-*λ*-0.75 changes. Due to the tearing of the joints between the upper concrete batten and the CFST limbs, the shear force of specimen S1-*λ*-0.75 could not be transferred; therefore, the shear strain curve rebounded.

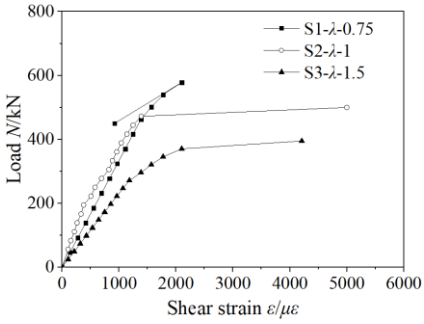

Fig. 4 Load-shear strain curve

4. Numerical simulation analysis

4.1. Establishment of the model

Finite element simulation is a widely adopted method for simulating the stress and deformation behavior of structures under varied conditions, allowing for the convenient analysis of diverse structural parameters. Software applications, including but not limited to ABAQUS, ANSYS, and MARC, have significantly augmented theoretical analysis and engineering practice related to these structures. Owing to the relatively high production difficulty and testing costs associated with the experimental model of steel tube concrete composite columns, further exploration of the structure's failure mechanisms and governing physical laws is warranted. ABAQUS software was employed to carry out simulation and analysis of the composite column. It was observed that the contribution of the transverse reinforcement pipe to the overall shear capability of the composite column was marginal. To enhance computational efficiency, a half-model of the steel tube concrete composite column structure was simulated, as depicted in Fig. 5.

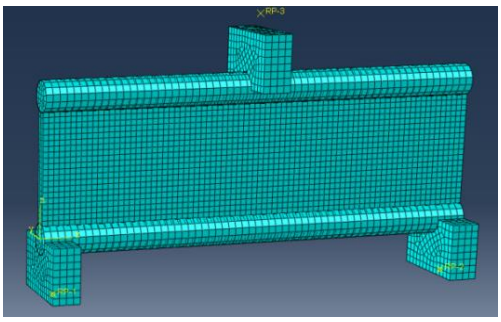

Fig. 5 Finite element test model

To simulate realistic boundary conditions, a vertical Z-directional load is applied to the composite column from the upper loading device. The displacements in the X and Y directions of the loading device are constrained. Additionally, both bottom supports of the lower two support devices are set as fixed.

The connection between the upper loading device and the lower support devices with the steel tubes employs a surface-to-surface contact approach, designating the loading apparatus or support devices as the primary face and the steel tubes as the secondary face. Normal contact is specified as "hard contact," and tangential contact is modeled using the Coulomb friction model with a friction coefficient set to 0.15 [1].

The interface between the core concrete enclosed by the steel pipe utilizes a surface-to-surface contact approach, designating the steel pipe as the primary face and the core concrete as the secondary face. The normal contact is characterized as "hard contact," and the simulation of tangential contact employs the Coulomb friction model with a friction coefficient established at 0.6 [18]. The linkage between the batten concrete and the steel pipe is classified as "Tie," and the batten steel bars are situated within the "embedded region" of the batten concrete.

To more precisely replicate mechanical responses, including tensile cracking and concrete material crushing within steel tube concrete, researchers both at home and abroad frequently adopt the concrete damage plasticity model.

Following comparative calculations across different constitutive models, the selection ultimately favored the constrained concrete constitutive model proposed by Liu Wei, as delineated in Eq. (1).

$$\begin{cases} \sigma = \sigma_0[2\frac{\varepsilon}{\varepsilon_0} - (\frac{\varepsilon}{\varepsilon_0})^2] & (0 < \varepsilon \le \varepsilon_0) \\ \sigma = \sigma_0(\frac{\varepsilon}{\varepsilon_0})\frac{1}{\beta(\frac{\varepsilon}{\varepsilon_0}-1)^2 + (\frac{\varepsilon}{\varepsilon_0})} & (\varepsilon > \varepsilon_0) \end{cases} \quad (1)$$

$$\sigma_0 = f_c^{'} \qquad \varepsilon_0 = \varepsilon_c + 800\xi^{0.2}$$

$$\varepsilon_c = 1300 + 12.5 f_c^{'}$$

$$\beta = 0.5 \times (2.36 \times 10^{-5})^{[0.25+(\xi-0.5)^7]} (f_c^{'})^{0.5} \ge 0.12$$

The upper loading device and the two lower support devices are both represented as rigid body elements. The batten concrete was simulated using C3D8 solid elements, while the batten reinforcement was represented by T3D2 truss elements. The steel pipe was modeled using S4 shell elements. The damage plastic model was used for the battened concrete and core concrete, and the steel material was characterized using a bilinear elastic-plastic constitutive model [22], as shown in Figs. 6 and 7.

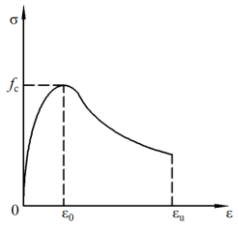

Fig. 6 Constitutive model of concrete

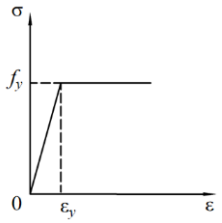

Fig. 7 Constitutive model of steel

4.2. Model validation

Comparisons between the calculated curves and experimental curves are presented in Fig. 8. The calculation curves closely align with the test curves, demonstrating a substantial overlap. It is noteworthy that only in the case of test S1-λ-0.75 did the ultimate load-bearing capability precede the simulation; nevertheless, the initial loading phase exhibited good concordance between the test and calculation curves.

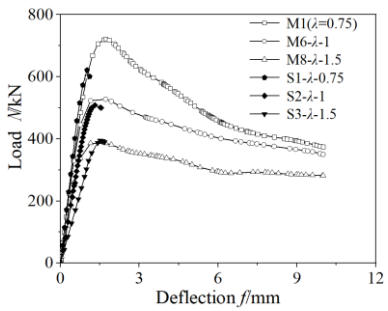

Fig. 8 Load-deflection comparison diagram of test and simulation

The discrepancy observed in S1-λ-0.75 can be attributed to the higher strength of the connection between the simulated finite element column limbs and the concrete batten, as compared to the actual specimen. Thus, shear failure under oblique compression was the failure mode rather than local shear failure. The results of the deviation analysis indicate the imperative need to enhance the connection between the column limbs and concrete batten, especially in cases with a small shear-span ratio. Furthermore, the results suggest a good correlation between the simulation and experiments, allowing for further parameter analysis based on this FEM.

The deviation analysis results show that it is necessary to strengthen the connection of the column limbs and concrete batten with a small shear-span ratio and indicate that the simulation could provide a reasonable estimation of the shear process of composite columns if the composite columns were inclined to experience compression shear failure.

4.3. Stress analysis

Display the stress maps for the principal tensile and compressive stresses of concrete and steel in Figs. 9 and 10, respectively.

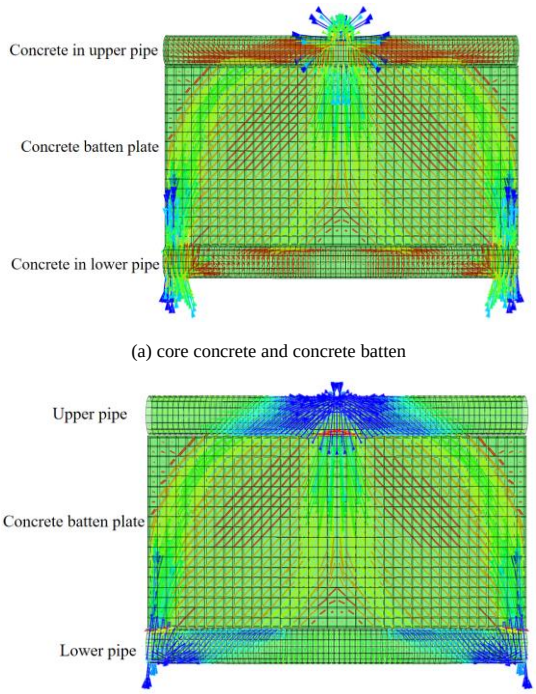

(a) core concrete and concrete batten

(b) steel pipes and concrete batten

Fig. 9 Direction of principal compressive stress

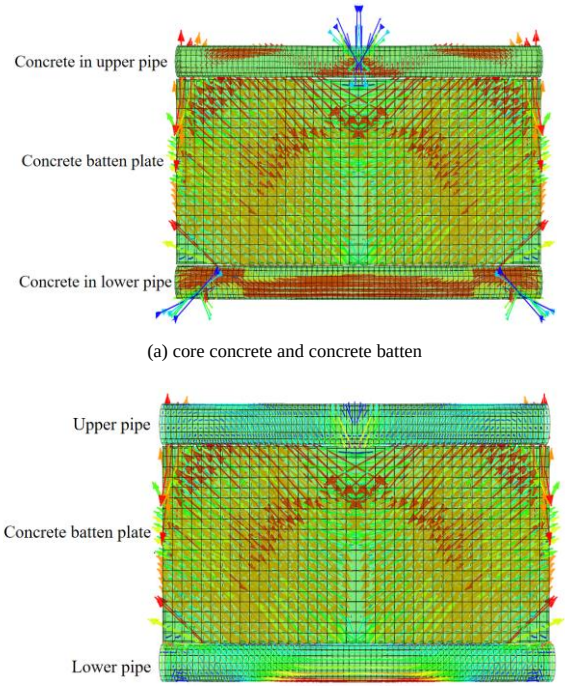

(a) core concrete and concrete batten

(b) steel pipes and concrete batten

Fig. 10 Direction of principal tensile stress

In addition to the stress flow disorder at the loading point and the supports, the distribution of the principal compressive and tensile stress in the other areas of the upper and lower steel pipes presented good regularity, which could connect with the stress distribution of the concrete batten well, indicating that the shear force could transfer between the steel pipe and the batten plate concrete.

The main pressure and tensile stress flow of the concrete in pipes were relatively disordered due to the circular action of steel pipes. According to the load path method, the main compressive stress area in the same direction was equivalent to the compression bars and the main tensile stress area in the same direction was equivalent to the tension bars. In this way, the strut-and-tie model of composite columns was formed.

In this model, the concrete diagonal strut was equivalent to the pressure bars of the strut-and-tie model and the shear force of the upper and lower steel tubes was transferred to the supports through the concrete diagonal struts. The tension side of the CFST acted as tension bars, ensuring equilibrium with the horizontal force exerted by the diagonal compression bars.

4.4. Parameter analysis

With the verified FEM, the strength of the batten concrete f_c (20 MPa ~ 50 MPa), shear-span ratio of the batten concrete λ (0.5~1.75), the thickness span ratio of the concrete batten t_c/L (0.033~0.073) and the outer diameter of the column limbs D (90 mm~240 mm) were analyzed. The parameters of each FEM are illustrated in Table 3.

Table 3
Basic parameters of finite element analysis

Specimens number	The strength of batten plate concrete/MPa	The width of barren plate b/mm	Shear-span ratio λ	The thickness of batten plate t_c/mm	Thickness span ratio t_c/L	The outer diameter of column limbs D/mm	V_{FEM}	$V_{c\text{-}China}$/kN	$V_{c\text{-}Simple}$/kN
M1	30	1000	0.75	50	0.033	114	721.2	1005	651.6
M2-f_c-30	20	1000	0.75	50	0.033	114	565.2	670	547.7
M3-f_c-40	40	1000	0.75	50	0.033	114	838.8	1340	739.1
M4-f_c-50	50	1000	0.75	50	0.033	114	920.8	1620	816.2
M5-λ-0.5	30	1500	0.5	50	0.033	114	1028	1507.5	922.1
M6-λ-1	30	750	1	50	0.033	114	527.6	753.75	516.3
M7-λ-1.25	30	600	1.25	50	0.033	114	457.2	603	435.1
M8-λ-1.5	30	500	1.5	50	0.033	114	385.6	502.5	381.0
M9-λ-1.75	30	428	1.75	50	0.033	114	345.2	430.14	342.0
M10-λ-2	30	375	2	50	0.033	114	316	376.87	313.3
M11-t_c/L-0.040	30	1000	0.75	60	0.040	114	788	1206	764.7
M12-t_c/L-0.047	30	1000	0.75	70	0.047	114	891.6	1407	877.9
M13-t_c/L-0.053	30	1000	0.75	80	0.053	114	994.8	1608	991.0
M14-t_c/L-0.06	30	1000	0.75	90	0.06	114	1107.2	1809	1104.2
M15-t_c/L-0.067	30	1000	0.75	100	0.067	114	1171.2	2010	1217.4
M16-t_c/L-0.073	30	1000	0.75	110	0.073	114	1301.6	2211	1330.5
M17-D-90	30	1000	0.75	50	0.033	90	640.4	-	610.2
M18-D-120	30	1000	0.75	50	0.033	120	688.4	-	664.7
M19-D-150	30	1000	0.75	50	0.033	150	784	-	749.5
M20-D-180	30	1000	0.75	50	0.033	180	888	-	870.3
M21-D-210	30	1000	0.75	50	0.033	210	1020	-	1032.6
M22-D-240	30	1000	0.75	50	0.033	240	1245.2	-	1241.4

In Table 11, specimen Model M1 is designated as the standard model with a concrete strength of 30 MPa, a concrete batten height of 1000 mm, a concrete batten thickness of 50 mm, and an outer diameter of column limbs measuring 114 mm. The corresponding load-deflection curves are depicted in Fig. 11.

Fig. 11(a) shows the load-deflection curves of CFST composite columns with different strengths of the concrete batten f_c. With increasing f_c, the ultimate shear capability of the composite columns increased obviously while the shear stiffness changed little. The model with f_c of 20 MPa was taken as the benchmark, and with increases in f_c from 20 MPa to 50 MPa in steps of 10 MPa, the ultimate shear capability of each step was increased by 39 kN (27.6%), 29 kN (16.3%) and 21 kN (9.8%). This analysis indicates that the reinforcement effect of increasing concrete strength on the ultimate shear capability of composite columns diminishes as the concrete strength rises. This observation suggests a nonlinear relationship between concrete strength and ultimate shear capability.

Fig. 11(b) illustrates the load-deflection curves of CFST composite columns with different shear-span ratios λ. With decreasing λ, the ultimate shear capability of CFST composite columns increased obviously while the shear bearing stiffness changed little. The model of λ value was equal to 2 was taken as the benchmark, and with decreases in λ from 2 to 0.5 in steps of 0.25, the ultimate shear capability of each step was increased by 7 kN (9.2%), 10 kN (11.7%), 18 kN (18.6%), 18 kN (15.4%), 48 kN (36.7%) and 77 kN (42.5%). The analysis revealed that the impact of the shear-span ratio on the shear capability of CFST composite columns intensifies as shear-span ratio decreases. This observation suggests a nonlinear relationship between shear-span ratio and shear capability.

Fig. 11(c) reveals the load-deflection curves of CFST composite columns with different thickness span ratios of the concrete batten t_c/L. With increasing t_c/L, the ultimate shear capability and the shear stiffness of the composite columns increased. The model with a t_c/L value of 0.033 was taken as the benchmark, and with increases in t_c/L from 0.033 to 0.073 in steps of approximately 0.07, the ultimate shear capability of each step was increased by 17 kN (8.5%), 26 kN (11.6%), 26 kN (10.4%), 28 kN (10.2%), 16 kN (5.5%) and 33 kN (10.0%). This analysis indicates that the impact of the thickness span ratio on the shear capability of CFST composite columns remains relatively constant with variations in the thickness span ratio. This suggests an almost linear relationship between the thickness span ratio and shear capability.

Fig. 11(d) shows the load-deflection curves of CFST composite columns with different outer diameters of column limbs D. The figure indicates that with increasing D, the ultimate shear capability of composite columns increased obviously. The model with a value of D of 90 mm was taken as the benchmark, and with increases in D from 90 mm to 240 mm in steps of 30 mm, the ultimate shear capability of each step was increased by 12 kN (7.0%), 24 kN (12.2%), 26 kN (11.7%), 33 kN (12.9%) and 56 kN (18.1%). This analysis reveals that the impact of the outer diameter of column limbs on the shear capability of composite columns becomes more pronounced with an increase in the outer diameter of the column limbs. This observation suggests a nonlinear relationship between the outer diameter of column limbs and shear capability.

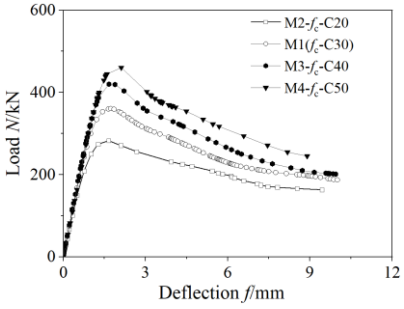

(a)The strength of batten concrete

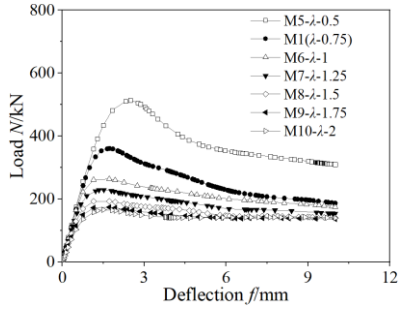

(b)Shear-span ratio

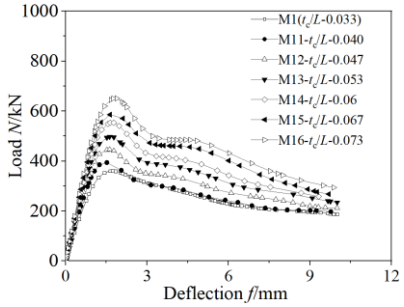

(c)Batten concrete thickness span ratio

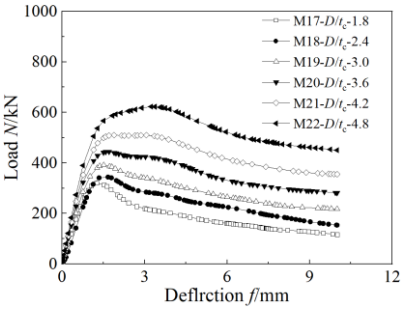

(d)The outer diameter of column limbs

Fig. 11 Load-deflection curves of CFST composite columns

5. Analysis of shear bearing performance

5.1. Accuracy evaluation of existing calculation methods

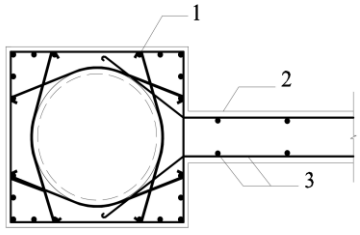

Fig. 12 CFST shear wall structure

1: End post; 2: Wall; 3 : Distributed reinforcement

Currently, there is a scarcity of research on the calculation methodology for the shear capability of CFST composites, both domestically and internationally. The “Technical specification for steel tube-reinforced concrete column structures” delineates a structure akin to that of a CFST shear wall, comprising a combination of a concrete-filled steel tube and a concrete shear wall, as depicted in Fig. 12.

The shear capability calculation method of this structure is illustrated in Eq. (1). This formula was used to calculate the CFST composite column, and the computed result was juxtaposed against the experimental value (finite element result), as illustrated in Fig. 13.

$$V_c \le 0.25\beta_c f_c b_w h_{w0} \quad (1)$$

V_c: the calculation value of the shear capability of the shear wall structure; f_c: the compressive strength of the shear wall concrete; b_w: the thickness of the shear wall; h_{w0}: the height of the shear wall; β_c: when the concrete strength is below 50 MPa, it is 0.5; when the concrete strength is above 80, it is 0.8.

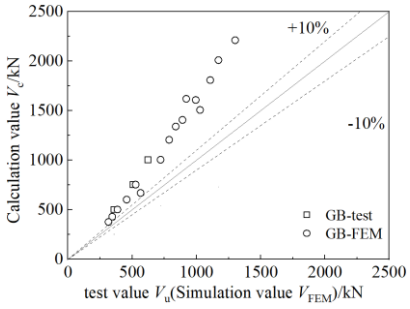

Fig. 13 Comparison diagram of formula calculation value and test value

Fig. 13 shows that although the CFST shear wall structure is very similar to the CFST composite column, the unique reinforced concrete outer layer of the shear wall structure will provide additional shear capability. Therefore, the calculation value obtained by this method is generally larger than the test value (finite element value), and this method is not suitable for the calculation of composite columns.

Investigation into the calculation methodology for the shear resistance capability of composite columns constitutes a crucial element in the safety assessment and structural design of such composite structures. By understanding the structural carrying capability under shear loads, adjustments to the dimensions, material selection, and construction methods of the structure can be made based on the calculated results. Therefore, it is necessary to design a calculation method that meets engineering precision requirements.

5.2. Calculation method

The test results in Section 1.4 are now analyzed. Firmly connecting the CFST column limbs with the concrete batten split the concrete batten was into several diagonal compression members, and the composite column reached the ultimate shear capability due to the diagonal compression shear failure of the concrete batten.

Due to the limited dataset available for analysis, this study exclusively focused on investigating the shear failure of the concrete batten in CFST composite columns, specifically identifying the failure mode as diagonal compression shear failure. The discussion of localized shear failure in joints has been reserved for subsequent research endeavors.

In alignment with the principal stress direction determined through the stress analysis in Section 2.3, the distribution of the principal stress direction in the concrete batten demonstrated a noteworthy regularity when the CFST composite column exhibited shear failure under oblique compression. Moreover, it was assumed that the diagonal compression bars formed during this failure mode could be considered parallel. Further in-depth exploration and discussion on this topic are anticipated in future studies.

Considering the restraint and load transfer effect of CFST on the concrete batten, the concrete batten and the lower concrete-filled steel pipes can be regarded as the strut-and-tie model of concrete beam shear failure [22], as illustrated in Fig. 14.

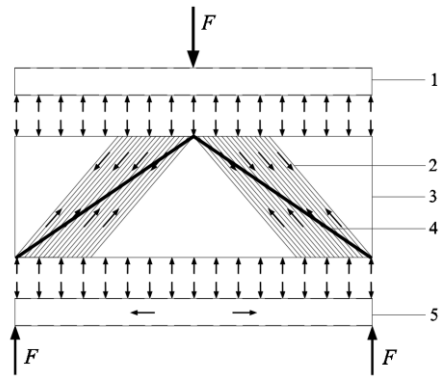

Fig. 14 Mechanism of shear capability of composite columns

1:Upper concrete-filled steel tubular columnar limb；2:Secondary pressure bars；3:Concrete batten plate；4:Main pressure bar；5:Lower concrete-filled steel tubular column limb

This model is different from the previous strut-and-tie model. The main compression bar connecting the loading center and the reaction center of the bearing can transfer the force. At the same time, due to the constraint of the CFST column at the bottom, the parallel secondary compression bars of the concrete batten can also transfer the force.

The composite column model was slightly different from the previous strut-and-tie model. The main compression bars connecting the loading point and the supports in the concrete infix plate can transmit force. Due to the component force of the top column limb and the restraint of the bottom column limb, the parallel secondary compression bars of the concrete batten can also transmit force [23].

Based on the strut-and-tie theory and the analysis of the influence of different outer diameters of column limbs D on the shear capability of composite columns in Section 2.4, the shear capability of CFST composite columns cannot be ignored.

Consequently, the culmination of the ultimate shear capability in the composite column is attributed to the collaborative effects of the main compression bars and secondary compression bars within the concrete batten, along with the CFST column limbs. The mathematical expression for calculating the shear ultimate load-bearing capability of CFST composite columns is delineated in Eq. (2).

$$V_{\mathrm{RC1}} = \frac{\xi_{\mathrm{b}}}{\xi_{\lambda} \tan\omega} f_{\mathrm{t}} t_{\mathrm{c}} b \tag{2}$$

V_{RC1}: the shear force transferred by the main compression bars;V_{RC2}: the shear force transferred by the secondary compression bars; V_{CFST}: the shear force transferred by the CFST column limbs.

5.3. Main compression model of the concrete

A full-length diagonal crack manifested along the line extending from the loading point to the supports, signifying the failure of the main compression bars. The main compressive stress diffused in the middle of the concrete batten, and the shape of the main compressive bars was similar to a bottle shape, as illustrated in Fig. 15.

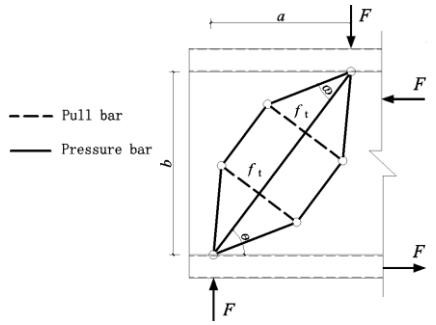

Fig. 15 Strut and tie model of main strut

In the CFST composite column, the failure of the main compression bars of the concrete batten was caused by the pull rod of the strut-and-tie model reaching the ultimate tensile capability.

The total shear force of the bottle-shaped compression bar model was defined as V_{RC1}. According to the analysis results of the strut-and-tie model in reference, the load-bearing capability of this part can be calculated by Eqs. (3)-(5).

$$V_{\mathrm{RC1}} = \frac{\xi_{\mathrm{b}}}{\xi_{\lambda} \tan\omega} f_{\mathrm{t}} t_{\mathrm{c}} b h \tag{3}$$

$$\xi_{\mathrm{b}} = 1.3 - 0.075 b / t_{\mathrm{c}} \quad (0.6 \le \xi_{\mathrm{b}} \le 1) \tag{4}$$

$$\xi_{\lambda} = \frac{1}{2.5 - \lambda} \quad (0.5 \le \xi_{\lambda} \le 1) \tag{5}$$

ξ_{b}: the impact of height thickness ratio on tensile strength of the concrete batten; ξ_{λ}: the influence coefficient of shear-span ratio on shear transfer path; f_{t}: the axial tensile strength of the concrete batten and can be calculated by $0.4 f_{\mathrm{c}}^{0.5}$;f_{c}: axial compressive strength of the concrete batten;b: the width of the concrete batten; t_{c}: the thickness of the concrete batten; ω: the diffusion angle of the main compression bars and compression bars with the shear force transferred indirectly; λ: shear-span ratio.

5.4. Secondary compression model of the concrete batten

The simplified model of the diagonal compression field of the concrete battened secondary compression bars is illustrated in Fig. 16. Through the equilibrium condition, the derivation of the calculation method for the load-bearing capability of the secondary strut is encapsulated in Eq. (6):

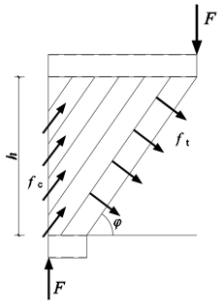

Fig. 16 Diagrammatic diagram of calculation of diagonal compression field model of secondary compression bar

$$V_{\mathrm{RC2}} = f_{\mathrm{t}} t_{\mathrm{c}} b h \cos\varphi / \sin\varphi \tag{6}$$

φ: the angle between secondary oblique pressure bars (zones) and horizontal direction in baroclinic field model, and it has a value of 45°; σ_{c} : the compressive stress of the secondary oblique pressure bars (zones) in the baroclinic field model; σ_{t} : the tensile stress between each diagonal compression bars(zones).

5.5. Calculation method for the shear capability of CFST column limbs

The shear capability calculation method for CFST column limbs, as detailed in references [24-25] and expressed in Eqs. (7)-(8), was employed. The computed shear capability of the column limbs was then juxtaposed with the shear capability of the concrete batten. The comparison included experimental and finite element values, and the results are depicted in Fig. 17.

$$V_{\mathrm{uCFST}} = 0.71 f_{\mathrm{sc}} A_{\mathrm{sc}} \tag{7}$$

$$f_{\mathrm{sc}} = 1.547 f \frac{\alpha_{\mathrm{sc}}}{\alpha_{\mathrm{sc}} + 1} \tag{8}$$

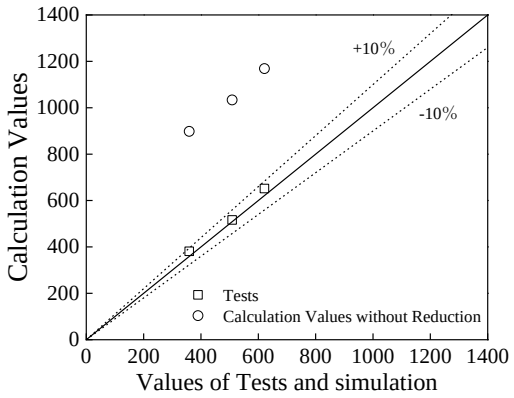

Fig. 17 Comparison chart of concrete filled steel tubular shear without reduction

Based on the examination of the test failure phenomenon and the findings illustrated in Fig. 17, it was observed that upon reaching the ultimate shear capability, the concrete batten exhibited cracking and crushing, while the CFST column limbs did not reach the shear limit. This observation suggests that the shear capability of the CFST column limbs was not fully utilized. Consequently, a reduction factor is incorporated into the calculation method for the ultimate shear capability of column limbs in composite columns, as delineated in Eqs. (9)-(10).

$$V_{\mathrm{CFST}} = \mu V_{\mathrm{uCFST}} \tag{9}$$

$$\mu = V_{\mathrm{CFST}} / V_{\mathrm{uCFST}} \tag{10}$$

V_{uCFST}: the shear capability of CFST; f_{sv}: the shear strength of CFST; A_{sc}: the sectional area of CFST; α_{sc}: the steel ratio of CFST; f_{sc}: the design value of compressive strength of steel; μ: the reduction factor of the shear capability of CFST column limbs, which can be calculated by Eq. (9); V_{CFST}: obtained by extracting the finite element values of the shear capability of the column limbs.

The shear capability of CFST column limbs has a high correlation with the outer diameter of the limbs *D*. With an increase in *D*, the reduction factor μ decreases, which indicated that the effect of *D* should be considered in the calculation of μ, as illustrated in Fig. 18.

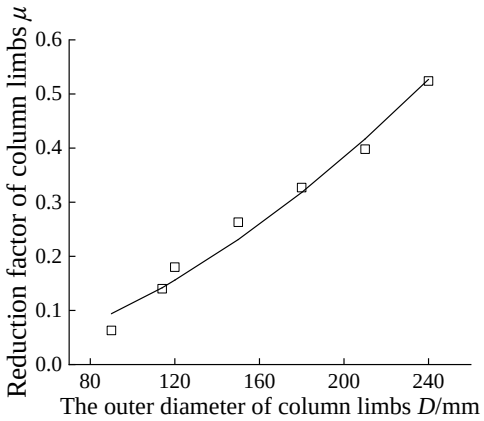

Fig. 18 Regression analysis of shear capability reduction factor

Through the regression analysis of *D* and μ, the relationship between them was calculated by Eq. (11).

$$\mu = 1.358\times10^{-4.6}\times D^{1.76} \tag{11}$$

5.6. Simplified calculation method

According to the American ACI code, if the main compression bars occur at the same time as the secondary compression bars, the minimum angle between the compression bar and the pull rod is 25° and shear-span ratio should be less than 2. If shear-span ratio was more than 2, then no main compression bars occurred in the concrete batten of the CFST composite column. The load was mainly transferred by the secondary compression bars. Therefore, the calculation method introduced in this study is applicable for cases in which shear-span ratio should be less than 2, as illustrated in Eq. (12).

$$V_{\mathrm{c}} = \frac{f_{\mathrm{t}} t_{\mathrm{c}} bh\cos\varphi_1}{\sin\varphi_1} + \frac{\xi_{\mathrm{b}}}{\xi_\lambda \tan\alpha} f_{\mathrm{t}} t_{\mathrm{c}} bh + 0.71\mu f_{\mathrm{sv}} A_{\mathrm{sc}} (\lambda < 2) \tag{12}$$

Eq. (12) is too tedious to apply to engineering applications; therefore, this paper carries out a simplified analysis of this formula. Eq. (9) and Eq. (12) show that parameters f_{t}, t_{c} and *h* were common between the calculation methods for the shear capability of the shear force V_{RC1} transmitted by the main compression bars and the shear force V_{RC2} transmitted by the secondary compression bars. After extracting the common factors, the following Eq. (13) can be obtained.

$$\begin{aligned} V_{\mathrm{c}} &= V_{\mathrm{RC1}} + V_{\mathrm{RC2}} + V_{\mathrm{CFST}} \\ &= \left(\frac{\cos\varphi_1}{\sin\varphi_1} + \frac{\xi_{\mathrm{b}}}{\xi_\lambda \tan\alpha}\right) f_{\mathrm{t}} t_{\mathrm{c}} bh + 0.71\mu f_{\mathrm{sv}} A_{\mathrm{sc}} \\ &= \kappa f_{\mathrm{t}} t_{\mathrm{c}} b + 0.71\mu f_{\mathrm{sv}} A_{\mathrm{sc}} \ (\lambda < 2) \end{aligned} \tag{13}$$

A good linear relationship is observed between κ and λ, as illustrated in Fig. 19. A regression analysis was performed, and the relationship between κ and λ is illustrated in Eq. (14)

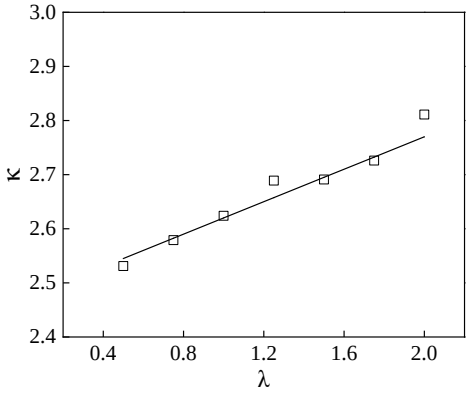

Fig. 19 Regression analysis of parameters of practical calculation formula

$$\kappa = (0.15\lambda + 2.47) \tag{14}$$

5.7. Verification of the calculation method

The parameters setting and shear capability of the tests and simulation models involved in this paper were illustrated in table1 and table 3. The calculated values obtained according to the calculation method in this paper are compared with the test values or simulation values of similar structures of many scholars, as illustrated in Fig. 20.

Comparisons between the calculated value and the experimental value (Simulation value) are illustrated in Table 2 (Table 3) and Fig. 20. The figure shows that the discrete points composed of the test value (finite element value) and the calculated value obtained by the strut-and-tie theory calculation method and the simplified practical calculation method basically fell near the straight line of V_{c}=V_{u} (V_{FEM}) and the deviation was generally controlled within 10%.

The data presented in Tables 2 and 3 demonstrate that the average ratios between the test values and the calculated values obtained through the strut-and-tie theory calculation method and the simplified practical calculation method are 1.007 and 1.038, respectively. Their respective standard deviations are 0.023 and 0.020. These results indicate a close agreement between the theoretical and simplified calculation values with the test values, underscoring the high accuracy of the proposed methods in this paper.

This paper introduces theoretical and simplified calculation methods that meet engineering precision requirements. These methods allow designers to

adjust the dimensions, material selection, and construction methods of the structure based on the calculation results, thereby reducing engineering costs. Simultaneously, in the simplified calculation method, the complexity of the calculations is reduced through a fitting process, resulting in models that are easier to understand or analyze. While ensuring the safety of structural design, this significantly enhances the efficiency of load-bearing capability calculations.

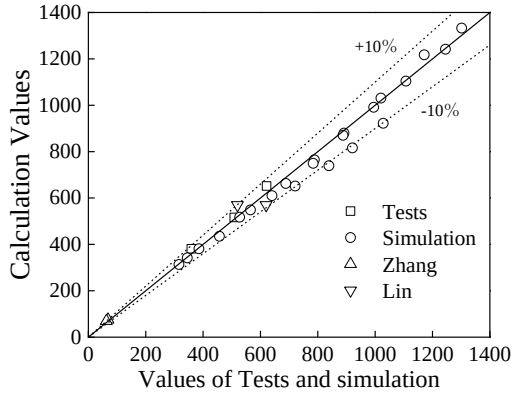

(a) Comparison of theoretical calculation methods

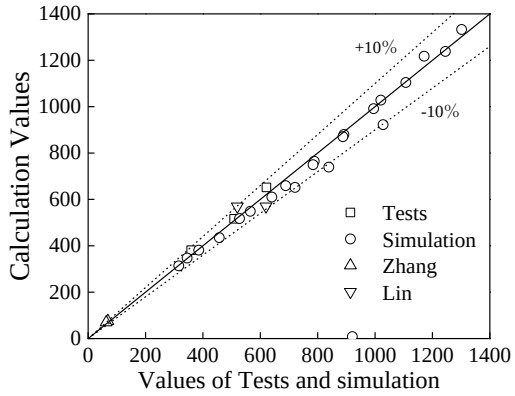

(b) Comparison of simplify calculation methods

Fig. 20 Comparison diagram of formula calculation value and test value

6. Conclusions

This study encompassed shear performance tests of CFST composite columns with varying shear-span ratios, finite element expansion parameter analyses, and an investigation into the load-bearing capability calculation method. The key findings are summarized as follows:

(1) The shear failure mode of CFST composite columns falls into two categories: shear failure under oblique compression and localized failure. The former is typic ally characterized by multiple shear diagonal cracks in concrete battens, more common in composite columns with larger shear-span ratios. The latter is typified by concrete spalling at the junctures of column limbs and concrete battens, often observed in composite columns with smaller shear-span ratios and a less firm connection between column limbs and concrete battens. The load-deflection curves of CFST composite columns are segmented into three stages: elasticity, plasticity, and declining load-bearing capability.

(2) The FEMs constructed in this study accurately simulated the entire shear failure process of CFST composite columns. The findings demonstrated that the shear capability of CFST composite columns escalates with the rise in batten concrete strength and thickness span ratio. Nevertheless, augmenting the outer diameter of the column limbs leads to a more pronounced enhancement in the shear capability of composite columns. Notably, composite columns demonstrate an increased shear capability when the shear-span ratio is minimized, contingent upon a robust connection between the column limb and batten. Therefore, enhancing the thickness span ratio of the batten concrete or the outer diameter of the column limbs can optimize the shear performance of CFST composite columns.

(3) Based on the analysis of CFST composite columns and the strut-and-tie model of the batten concrete, the ultimate shear capability of CFST composite columns is provided by the primary and secondary compression bars of the concrete batten and the CFST column limbs. Additionally, the reduction factor of CFST column limbs was calculated. Ultimately, the theoretical and simplified practical calculation methods, more accurate than the existing calculation methods for similar structures, were established. The deviation in these two calculation methods can be confined to within 10%, rendering the proposed method a reliable reference for the engineering application of CFST composite columns.

Acknowledgments

The research presented in this paper was supported by the National Natural Science Foundation of China (Grant No. 51578756) and by the Program for Innovative Research Teams in Science and Technology in Fujian Province University. The support is gratefully acknowledged.

References

[1] Baltay, P. and Gjelsvik, A. Coefficient of friction for steel on concrete at high normal stress. Journal of Materials in Civil Engineering, 1990, 2(1): 46-49.
[2] Chen, B.C. and Wang, T. Overview of concrete filled steel tube arch bridges in China. Practice Periodical on Structural Design and Construction, ASCE, 2009, 14(2):70-80.
[3] Chen, B.C., Yan, Q.L. and Xue, J.Y. Experimental study on compressive property of concrete-filled steel tubular hybrid stub columns. Journal of Building Structures, 2017, 37(5):82-91.
[4] Chen, B.C., Lai, Z. C., Yan, Q. L., Amit, H. Varma. Experimental behavior and design of CFT-RC short columns subjected to concentric axial loading. Journal of Structural Engineering, 2017, 143 (11) :04017148.
[5] Ou, Z.J. and Chen, B.C. Experimental research on influence of eccentrically ratio on concrete filled steel tubular laced columns compressed eccentrically. Journal of Building Structures, 2007, 28(S1):184-190.
[6] Zhang, W., Chen, Z., Xiong, Q. Performance of L-shaped columns comprising concrete-filled steel tubes under axial compression [J]. Journal of Constructional Steel Research, 2018, 145: 573-590.
[7] Xiong Q, Zhihua C, Jingfu K, et al. Experimental and finite element study on seismic performance of the LCFST-D columns [J]. Journal of Constructional Steel Research, 2017, 137(oct.): 119-134.
[8] Xiong Q, Chen Z, Zhang W, et al. Compressive behaviour and design of L-shaped columns fabricated using concrete-filled steel tubes [J]. Engineering Structures, 2017, 152(dec.1): 758-770.
[9] Yong, X., Li, X.L. Experimental study and numerical analysis on seismic behaviors of RC frame- frame truee composite wall. Chinese Journal of Applied Mechanics, 2024, 1-10.
[10] Yadav, R., Chen, B.C., Yuan, H.H., Lian, Z.B. Experimental investigation of CFST-RC bridge piers under cyclic loading. Procedia Engineering.2017, 173: 1723- 1730.
[11] Yadav, R., Chen, B.C., Yuan, H.H., Lian, Z.B. et al. Effect of width of RC-web on seismic performance of CFST–RC pier: experiments. Iranian Journal of Science and Technology, Transactions of Civil Engineering, 2019, 43:685-696.
[12] Yadav, R., Chen, B.C., Yuan, H.H., Lian, Z.B. et al. Analytical behavior of CFST bridge piers under cyclic loading. Procedia Engineering, 2017, 173:1731-1738.
[13] Zhou, J., Li, P., Guo, N.F. Seismic performance assessment of a precast concrete-encased CFST composite wall with twin steel tube connections. Engineering Structures, 2020, 207: 110240.
[14] Zhang, J., Li, X., Yu, C., Cao, W. Cyclic behavior of high-strength concrete shear walls with high-strength reinforcements and boundary CFST columns. Journal of Constructional Steel Research, 2021, 182: 106692.
[15] Fan, J.S., Liu, C., Yang, Y., Bai, Y., Wu, C. Shear capability of 3D composite CFT joints subjected to symmetric loading condition. Journal of Constructional Steel Research, 2015, 112: 242-251.
[16] Wei, J.G., Luo, X., Lai, Z.C., Amit, H. Varma. Experimental behavior and design of high-strength circular concrete-filled steel tube short columns. Journal of Structural Engineering (ASCE), 2020, 146(1): 04019184-1-16.
[17] Yan, Q. L. Research on the Ultimate Load Carrying Capability of Concrete-filled Steel Tubular Composite and Hybrid Columns. Ph.D. Dissertation, Fuzhou University, Fuzhou. 2017.
[18] Olofsson, U. and Holmgren, M. Anvandning av en servo-hydraulisk drag- vridningsmaskin for friktionsmatning mellan stal och betong vid laga glidhastigheter. Swedish National Testing and Research Institute, Boras, Sweden. 1992.
[19] Wu, Q.X., Huang, Y.F., Chen, B.C. Nonlinear aseismic performance of lightweight bridge with CFST composite truss girder and lattice pier. Engineering Mechanics, 2015, 32 (12) :90-98+116.
[20] Wang, J. J., Nie, X., Bu, F. M., Tao, M. X., & Fan, J. S. Experimental study and design method of shear-dominated composite plate shear walls. Engineering Structures, 2020, 215: 110656.
[21] Liao Y.B., Experiment and research on concrete filled steel tubular laced columns under axial compression, Tsinghua University, Beijing. 2009.
[22] Liu, W. Research on Mechanism of Concrete-Filled Steel Tubes Subjected to Local Compression. Ph.D. Dissertation, Fuzhou University, Fuzhou. 2005.
[23] Lin, Y. Experimental investigation and finite element analysis of RC simply supported deep beam. Hunan University, Hunan. 2011.
[24] Zhang, X.J. and Hu, X.S. Analysis for Shear Sterength of Reinfored Concrete Framed Columns. WuHan Urban Consteuction Institute. 1995(12).
[25] Wang, M.P. and Wang, X.T. Shear strength calculation of reinforced concrete beams with small shear-span ratio. Journal of Building Structures, 1996(05):73-78.